REPORT DOCUMENTATION PAGE

Form Approved
OMB No. 0704-0188

1. AGENCY USE ONLY (Leave blank)	2. REPORT DATE	3. REPORT TYPE AND DATES COVERED
	Feb. 8, 1995	Final, 5/13-11/13/94

4. TITLE AND SUBTITLE

Development of a Novel Wind Lidar

5. FUNDING NUMBERS

C:F49620-94-C-0052

6. AUTHOR(S)

H. Sang Lee

AFOSR-TR-95-0177

7. PERFORMING ORGANIZATION NAME(S) AND ADDRESS(ES)

Science & Engineering Services, Inc.
4014 Blackburn Ln.
Burtonsville, MD 20866

8. PERFORMING ORGANIZATION REPORT NUMBER

AF-94-1

9. SPONSORING/MONITORING AGENCY NAME(S) AND ADDRESS(ES)

USAF/AFMC
Air Force Office of Scientific Research
110 Duncan Av. Ste. B115
Bolling AFB DC 20332-0001

10. SPONSORING/MONITORING AGENCY REPORT NUMBER

11. SUPPLEMENTARY NOTES

12a. DISTRIBUTION/AVAILABILITY STATEMENT

Approved for public release; distribution unlimited.

12b. DISTRIBUTION CODE

13. ABSTRACT *(Maximum 200 words)*

A prototype new incoherent Doppler lidar system was designed for atmospheric wind measurements with a high accuracy up to a 5 kilometer slant path range in Phase I. This sensor is based on the pseudo-random modulation cw lidar technique in conjunction with a new incoherent Doppler lidar method, in which the return PRM laser signal is passed through a Doppler filter before being digitally processed to determine range resolved wind velocity in real time. Extensive simulation study shows, in the baseline system configuration with a 50 cm receiver and one watt transmitter power, a 200 seconds' signal integration will provide the required signal to noise ratio for a few percent accuracy measurement which corresponds to 1 m/s accuracy over a 50 m/sec dynamic range. Our Phase I experiment provided a unique technology basis for the construction of a high power narrow linewidth SLM diode laser system for cost effective and robust PRM laser transmitter. Consisting of the transmitter module, solid etalon based Doppler filter module, PRM data module and a receiver module, the sensor will be compact and lightweight with low power consumption and low cost. The sensor will be intrinsically insensitive to noise, background radiation, and other system bias.

14. SUBJECT TERMS

PRM Wind Lidar, Incoherent Doppler, Diode Laser

15. NUMBER OF PAGES

34

16. PRICE CODE

17. SECURITY CLASSIFICATION OF REPORT	18. SECURITY CLASSIFICATION OF THIS PAGE	19. SECURITY CLASSIFICATION OF ABSTRACT	20. LIMITATION OF ABSTRACT
Unclassified			

Development of a Novel Wind Lidar

Final Report
on SBIR Phase I

Contract #: F49620-94-C-0052

Science & Engineering Services, Inc.
4040 Blackburn Ln., Ste. 105
Burtonsville, MD 20866

Feb. 7, 1995

Abstract

A prototype new incoherent Doppler lidar system was designed for atmospheric wind measurements from the ground based platform with a high accuracy up to a 5 kilometer slant path range in Phase I. This sensor is based on the pseudo-random modulation cw lidar technique in conjunction with a new incoherent Doppler lidar method, in which the return PRM laser signal is passed through a Doppler filter before being digitally processed to determine range resolved wind velocity in real time. Extensive simulation study shows, in the baseline system configuration with a 50 cm receiver and one watt transmitter power, a 200 seconds' signal integration will provide the required signal to noise ratio for a few percent accuracy measurement which corresponds to 1 m/s accuracy over a 50 m/sec dynamic range. Our Phase I experiment provided a unique technology basis for the construction of a high power narrow linewidth SLM diode laser system for cost effective and robust PRM laser transmitter. Consisting of the transmitter module, solid etalon based Doppler filter module, PRM data module and a receiver module, the sensor will be compact and lightweight with low power consumption and low cost. In this novel configuration, the sensor will be intrinsically insensitive to noise, background radiation, and other system bias, thereby performing autonomous and maintenance-free operations. The PRM wind lidar system has a large commercial potential for real time wind profile measurements near airports to improve the avionic safety at landing and takeoff by nowcasting hazardous wind conditions. In addition to the avionic applications, the sensor will satisfy a number of requirements in the battlefield concerning the trajectory calculations as well as the forecast of the bio-chemical warfare dispersion.

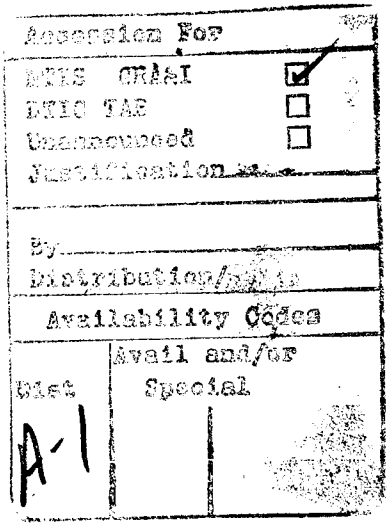

Table of Contents

1. Introduction/Summary

Phase I study concerns three major objectives concerning the development of a novel PRM wind lidar development including the system analysis, laser transmitter development, and feasibility experiments. The first objective is a detailed system analysis to quantify the performance of the baseline system under the normal environmental conditions. Toward this objective, we have developed an extensive computer simulation model which involves the propagation and backscattering of the PRM transmitter output in a standard atmosphere loaded with the standard aerosols model. The model then assumes a number of system parameters with which the received signal is quantified accurately. The simulated signal is then processed through the correlation operation, Doppler filter process and eventually for the wind speed measurement. The relevant background radiance level and all the system noise involved are also systematically implemented in the model. The validity of the model is cross checked by comparing the S/N ratios from both the model and the theoretical analysis.

The most important findings of the Phase I simulation study concerns the maximum range capability of the PRM lidar for the atmospheric measurement. Unlike the case of laser radar measurement for the hard target, the signal from the distributed targets, such as the atmosphere, consists of the return signals from the entire spatial extent at a given temporal point. Thus the photon statistical noise and its propagation in the measurement is significantly complex and different from that of conventional pulse lidar systems. As the details of this study is further discussed in Sec.3.1, the effect of the photon statistics noise in PRM system is significantly more pronounced than in the case of pulse lidar system and as a result the maximum range for the measurement becomes significantly limited. Furthermore, the increase of the transmitter power does not help to extend the ranges significantly. Thus the slant range coverage of PRM wind lidar is limited to about 5 km. Even with a substantial transmitter power increase, this range limitation is difficult to overcome. Nevertheless, the real time wind profile measurement range of 5 km can address a number of applications encompassing avionic safety applications, battlefield weather nowcast and trajectory calculations. Within these applications, the PRM wind lidar offers the best sensor solution with a large cost benefit and robust maintenance free operation for day and night over an extended period.

The second objective of Phase I is to develop a high power (~ 1 watt) narrow linewidth (< 15 Mhz) PRM modulated diode laser transmitter. Toward this objective, we have set up a laboratory breadboard diode Slave/Master Oscillator Laser (SMOL) system and demonstrated the injection locking of the modulated slave laser output frequency at a stable narrow line of the oscillator. This breadboard experiment is the first of a kind demonstration of the unique PRM transmitter and will be improved for a higher power in Phase II. Further details of this result is discussed in Sec.3.3 of this proposal. This result provides the basis of our selection of the best concept for the PRM laser transmitter. In addition to the simplicity and robust performance of the system, another important merit of this concept is the unlimited potential for the increased transmitter power. We envision scaling up the output power of the SMOL system by multiplexing high power diode lasers using the same oscillator and an array of beam splitters.

The third objective of Phase I is to perform a test bed experiment for Doppler measurement of a moving target in the laboratory. The purpose of the experiment is to get the first hand experience with the critical parameters of the system design and further identify the technology bases needed to be developed in Phase II. For this end, we have set up an experiment to measure the Doppler shift of the scattered diode laser beam from a rotating chopper with varying speed up to tens of m/sec. As further discussed in Sec.3.2, the preliminary result shows measurable sensitivity of our breadboard PRM system. Qualitative experiment is planned at present by characterizing the spectral parameters of the diode laser used and the solid etalon filter in order to quantify the stability of the spectral characteristics. The result of this experiment will be utilized for Phase II detailed design of the transmitter module and filter module. Based on the present transmitter development plan, we will be actively narrowing the transmitter linewidth to less than 15 Mhz, and the stability of the wavelength will be actively controlled using a feedback signal consisting of the transmittance of the laser through the actual filter in realtime.

2. Phase I Objectives

The proposed Phase I objectives are listed below verbatim as a reference to the review of the Phase I results.

The objective of the Phase I study is to demonstrate the feasibility of the PRM/Doppler wind lidar concept for atmospheric wind measurement with high resolution and sensitivity, and to further conceptualize the Phase II system. Specifically, the verification of compatibility of PRM with "edge technique" is the main Phase I objective. Proof of principle experiments for the compatibility will be conducted using a laboratory test bed. System analysis in terms of the signal to noise ratio analysis and performance characteristics will be performed. Parameters of the baseline configuration of the Phase II system will be defined, based on the performance analysis. Subsequent system level design of the sensor is planned in preparation to Phase II work. Further development, test, and prototyping of the sensor will follow in Phase II.

3. Phase I Results

In this section we discuss the Phase I results in detail especially in relation to the Phase II tasks proposed and further technology development. Through the Phase I study, we have developed a unique design feature of the wind lidar sensor to be developed in the following phase. The system is uniquely characterized as a compact field worthy system with a low power consumption and virtually no maintenance requirement on the ground based or airborne operations. Based on the Phase I study we have developed a sensor configuration summarized in Table 3.0.1. The details of the system design parameters for Phase II are further discussed later in this section.

In the following subsections, we first describe the simulation study results which outlines the overall configuration of the prototype system to be developed in Phase II.

Table 3.0.1 Proposed Baseline Sensor Configuration

Laser	AlGaAs Diode Laser	
	Wavelength	813 - 817 nm
	Linewidth	15 Mhz
	Power	> 1 W
	Beam Divergence	< 1 mrad
	Scan Resolution	~ 5 mrad
Time Resolution		< 100 nsec; Variable
Modulation: M-Sequence Pseudo-Random Code		
	Clock Time	Programmable for dt = 100 nsec, or
Number of Elements		N = 1023 (2^{10} -1)
	Period	102.3
Receiver Optics		
	Telescope	50 cm Dia.
	Interference Filter	~.1 nm FWHM
Edge Filter		Etalon
	HWHM	0.0023 cm^{-1}
	Finesse	30
Detector		
	SiAPD	Geiger Mode
	Quantum Efficiency	0.6
	Excess Noise Factor	9
	Preamplifier	Trans-impedance
Signal Processor		
	ADC	1 Bit Photon Counter
	Integrator	12 Bit, ~ 100 sec
	Computer	Micro-Computer
	Display	Color Graphics

3.1. Simulation of PRM Doppler Wind Lidar

The PRM lidar performance simulations make use of four different programs.

1) WVDEAP.FOR - Calculates the expected atmospheric response using the lidar equation and input system parameters. The addition of signal due to molecular scatter is disabled in the program (in subroutine OFFLIN.FOR.) The offline signal calculated in WVDEAP is written to an ascii file.

2) PRMCON.FOR - Convolves the expected atmospheric impulse response with the PRM code sequence, which with the addition of random noise and background signal, simulates the signal expected at the lidar receiver.

3) PRMCOR.FOR - Correlates the simulated received signal generated in PRMCON.FOR with the PRM code sequence.

4) SHOWNOIS.FOR - Calculates the percentage difference between the atmospheric impulse response, and the retrieved atmospheric response produced by PRMCOR.FOR. The random error component in the retrieved signal may then be estimated by examination of the result.

The expected impulse response is first simulated by a separate computer program (Dial Error Analysis Program) designed to predict signal levels from an atmospheric return using a pulsed lidar. The atmospheric impulse response is that received by the transmission of one 'on' bit of the PRM code sequence, where the bit energy is just the CW laser transmitter power times the duration of the bit (= inverse of the transmitter modulation frequency.)

The direct simulation of PRM lidar provides a quantitative estimate of the signal levels and uncertainty. This estimate is compared with the theoretical estimate of signal to noise derived

from Poisson statistics. In both cases, once the uncertainty of the PRM signal is estimated, the precision of the wind measurements is estimated based on the frequency characteristics of the filter function, which is used to convert the Doppler shift of the return signal to filter transmittance variation.

3.1.1. Principle of PRM Measurements

The PRM CW lidar relies on the delta function property of the autocorrelation function of a pseudo-random (PR) code. The CW diode laser output is modulated by an *N*-th order PR code and is transmitted as a continuous modulated signal train. The return signal from the target is a convolution of the transmitted signal x_i, and the impulse response function R_i, of the target [Takeuchi et al.], [Nagasawa et al.]

$$y(i) = \sum_{j=0}^{N-1} x_{i-j} R_j + b \tag{1}$$

The transmitted signal $x_i = P_o\, a_i$, where a_i is the PR code, P_o is the laser power, and b is the background level.

Retrieving the target impulse response function, whether a delta function from a hard target, or the distributed atmospheric response, requires correlating the received signal with the transmitted PR code. To perform the correlation, the PR code is modified so that the zeros are replaced with -1's. Then the cross-correlation of the original and modified codes gives the delta function.

$$C(j) = \sum_{i=0}^{N-1} a_i\, a'_{i+j} \tag{2}$$

Maximum-length (M) sequence codes are often used as PR codes and in this case the cross-correlation has the following value

$$C(j) = scalesym200\{ \begin{matrix} l & j=0 \\ 0 & j\neq 0 \end{matrix} \tag{3}$$

where $l=(N+1)/2$.

The M sequence code a_i', yields the target impulse response function $S(k)$, when correlated with the received signal.

$$S(k) = \sum_{i=0}^{N-1} y_i\, a'_{i-k} \tag{4}$$

since:

$$S(k) = \sum_{i=0}^{N-1} scalesym200\{ \sum_{j=0}^{N-1} x_{i-j} R_j + b_i scalesym200\} a'_{i-k} \quad (5)$$

$$= P_o \sum_{j=0}^{N-1} C(j-k) R_j + \sum_{i=0}^{N-1} a'_{i-k} b_i \quad (6)$$

It has been shown [Takeuchi et al.] that the SNR equation for the PRM lidar depends on the average value of the response function and the background level.

$$S/N = \frac{\sqrt{M}\sqrt{\xi}\, l P_o \Delta t\, r_j}{\sqrt{N}\sqrt{l P_o \Delta t\, \bar{r} + \bar{b}}} \quad (7)$$

where M is the number of code cycles accumulated (1 code cycle has N bits), ξ is the conversion factor for received power to photoelectrons. $R_j = r_j \Delta t$, where r_j is the average impulse response function over the modulation bin time Δt. $\bar{r}$ is the average impulse response over one code cycle, and $\bar{b}$ is the average background.

3.1.2 Simple Derivation of PRM Signal to Noise Expression

To derive the signal to noise expression, it is useful to view the atmosphere as acting like a source of N PRM code trains, each consecutive train offset in time by one bin width. The signal received at a given time is the sum of these code trains, which at time t_i have, on average, l 1's and l-1 0's, where $l = (N+1)/2$. The sum of the code trains, y_i, is the signal detected at the receiver at time bin i,

$$y_i = l\bar{A} + \bar{b} \quad (8)$$

where $\bar{A} = \xi P_o \Delta t\, \bar{r}$ is the average signal from the atmosphere per time bin per code train. The average background per bin is given by $\bar{b}$.

When performing the correlation, we sum y_i multiplied by either 1 or -1 over N time bins. The alignment of the multipliers depends on the offset lag of the correlation. We can separate out the contribution of the signal from a given part of the atmosphere, A_j, in describing the correlation S_j:

$$S_j = \sum_{i=0}^{l} [A_j + (l-1)\bar{A} + \bar{b}]_i - \sum_{i=l+1}^{N} [l\bar{A} + \bar{b}]_i \quad (9)$$

The first sum contains the l terms that have signal from the atmospheric bin Z_j, and the remaining l-1 terms have no contribution. Multiplying gives:

$$S_j = lA_i + l(l-1)\bar{A} + l\bar{b} - (l-1)l\bar{A} - (l-1)\bar{b} = lA_i + \bar{b} \quad (10)$$

Since calculating the correlation involves l additions and l-1 subtractions, the uncertainty in this calculation is the sum of the absolute value of each term (the sum of the squares of the uncertainty of each term, which is the square root of the magnitude of each.) The signal to noise of the correlation corrected for the background is:

$$S/N = \frac{lA_j}{\sqrt{lA_j + 2l(l-1)\bar{A} + N\bar{b}}} \tag{11}$$

Including the A_j in the average $\bar{A}$, gives $(2l-1)l\bar{A} = Nl\bar{A}$. The signal to noise for a single code cycle can be written as:

$$S/N = \frac{lA_j}{\sqrt{N}\sqrt{l\bar{A} + \bar{b}}} \tag{12}$$

3.1.3. Wind Measurement Uncertainty

The wind velocity u, measured as a function of the Doppler shift $\Delta\nu$ of the backscattered light is:

$$u = \frac{\lambda}{2}\Delta\nu \tag{13}$$

When the transmitting wavelength λ = 852 nm, a 1 m/s wind speed corresponds to a 2.35 Mhz Doppler shift. The uncertainty in the wind speed σ_u for an uncertainty in the Doppler shift $\sigma[\Delta\nu]$ or for a single frequency measurement of uncertainty σ_ν is:

$$\sigma_u = \frac{\lambda}{2}\sigma[\Delta\nu] \approx \lambda\,\sigma_\nu \tag{14}$$

The uncertainty in the frequency of the return signal in terms of the signal uncertainty σ_s after passing through the edge filter:

$$\sigma_\nu = \frac{\sigma_s}{\frac{\partial S}{\partial \nu}} \tag{15}$$

where the derivative is the slope of the filter function at the received wavelength.
The uncertainty in the wind velocity for a particular range bin j is:

$$(\sigma_u)_j = \frac{\lambda\sqrt{N}\sqrt{l\bar{A}\,T + \bar{b}}}{\sqrt{M}\,l A_j \frac{\partial T}{\partial \nu}} \tag{16}$$

where T is the transmission of the filter, and A_j is the atmospheric signal at the range of interest.

The filter transmission and the filter transmission gradient $\partial T/\partial\nu$ are calculated by convolving

a Lorentzian lineshape representing the laser emission with a sawtooth function representing the filter transmission function. A larger number for the transmission gradient obviously signifies a higher sensitivity to return signal frequency shifts. Table 3.1.1 gives the value for $\partial T/\partial \nu$ at various values of filter full scale half width (width of filter from $T=0$ to $T=1$), and laser line width.

Filter FSHW (Mhz)	Laser Line Width (Mhz)	$\partial T/\partial \nu$ High (10^{-9} Hz^{-1})	$\partial T/\partial \nu$ Low (10^{-9} Hz^{-1})
250	10	3.30	3.27
	50	2.36	1.81
	100	1.55	0.97
500	10	1.73	1.73
	50	1.48	1.45
	100	1.20	1.10
1000	10	0.88	0.88
	50	0.82	0.82
	100	0.74	0.74

Table 3.1.1. Values of filter transmission gradient for various values of filter width and laser HWHM. The high value has the laser line center at 50 Mhz inside the filter 50% transmission point, and the low value is with the laser line center positioned 50 Mhz outside the filter 50% transmission point. This represents the transmission gradient value over the full range of expected frequency shifts.

3.1.4 Estimated Wind Velocity Measurement Uncertainty

The parameters used in the simulation are given as follows: The average background for daytime, b = 24 counts/200 ns. The number bins N = 511 and l = 256. The filter transmission T = 0.40. The filter transmission gradient $\partial T/\partial \nu = 3.2 \times 10^{-9}$ Hz^{-1}. Transmission wavelength λ = 852 nm. The number of code cycles averaged $M = 1.96 \times 10^6$, or 200 sec accumulation at 5 Mhz modulation frequency. The transmitter power is 1 W. These parameters are also summarized in Table 3.1.2.

Table 3.1.3 shows the relative uncertainty in the retrieved signal intensity (S(k)) estimated for simulated PRM measurements of atmospheric impulse response from a ground-based Doppler PRM lidar. The four data sets correspond with the data given in the Figures 3.1.1-4. The figures show the error in the retrieved impulse response relative to the impulse response input into the simulations. The four situations are horizontal pointing with coaxial and biaxial alignment of the transmitter to the receiver optical axis, and vertical pointing with coaxial and biaxial alignment. The atmospheric impulse response for the coaxial and biaxial alignments is shown in Figure 3.1.5 for the vertical profile and in Figure 3.1.6 for the horizontal profile. Evidently, the horizontal profiles are more precise over a larger distance because of the smaller gradient in impulse response over range. The biaxial arrangement reduces the signal gradients by omitting the stronger portion of the near-field signal return. Equation 12 shows that the SNR depends on the average signal level as well as the signal level of the range bin of interest.

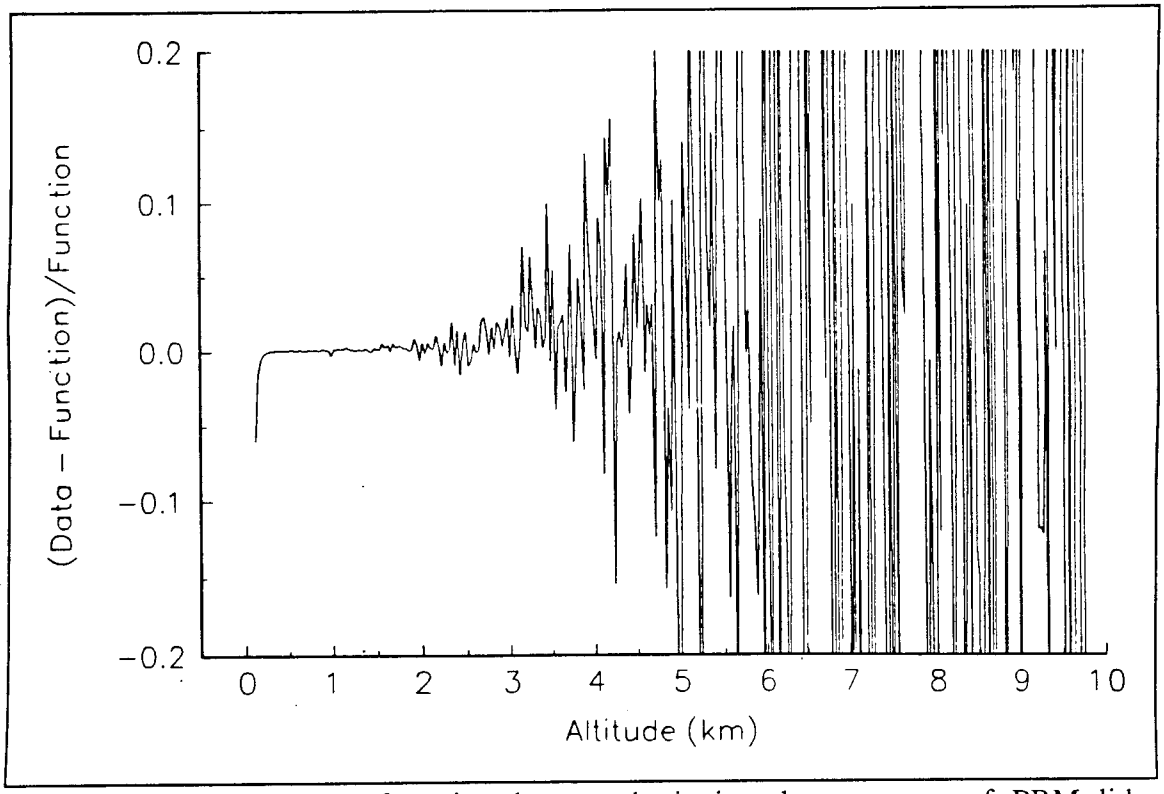

Fig. 3.1.1 Relative error of retrieved atmospheric impulse response of PRM lidar simulation. Vertical pointing with coaxial alignment.

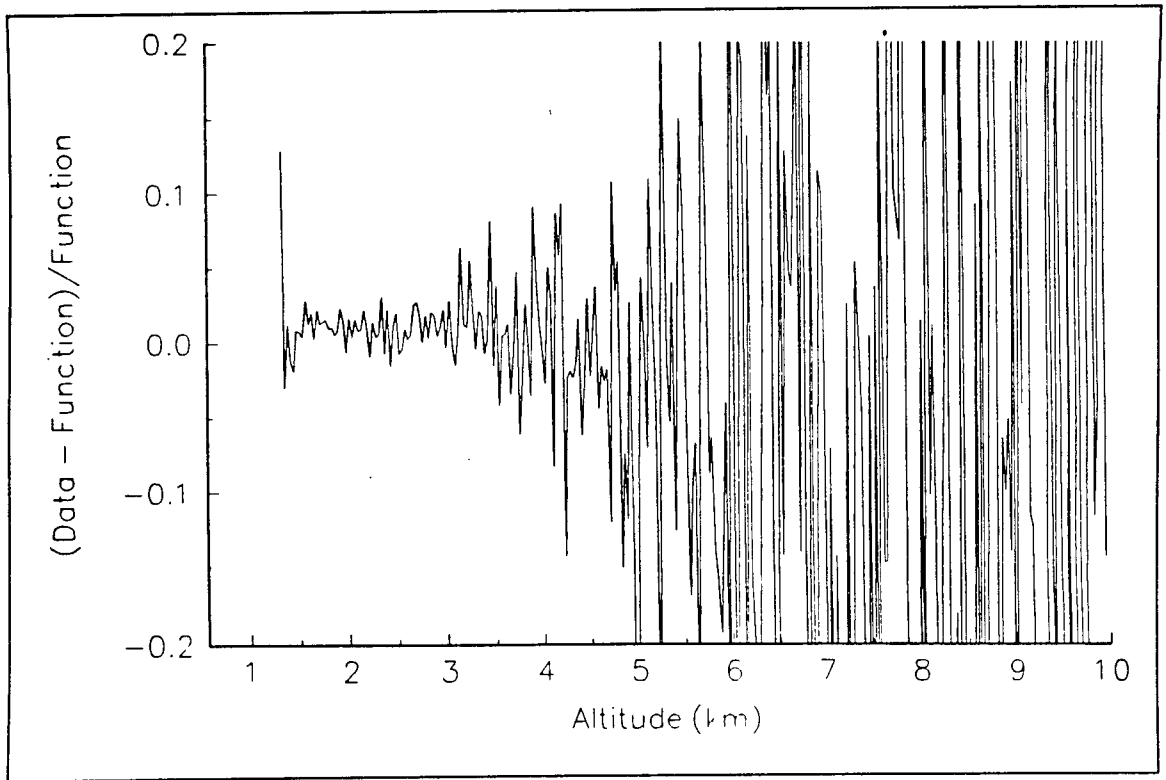

Fig. 3.1.2 Relative error of retrieved atmospheric impulse response of PRM lidar simulation. Vertical pointing with biaxial alignment.

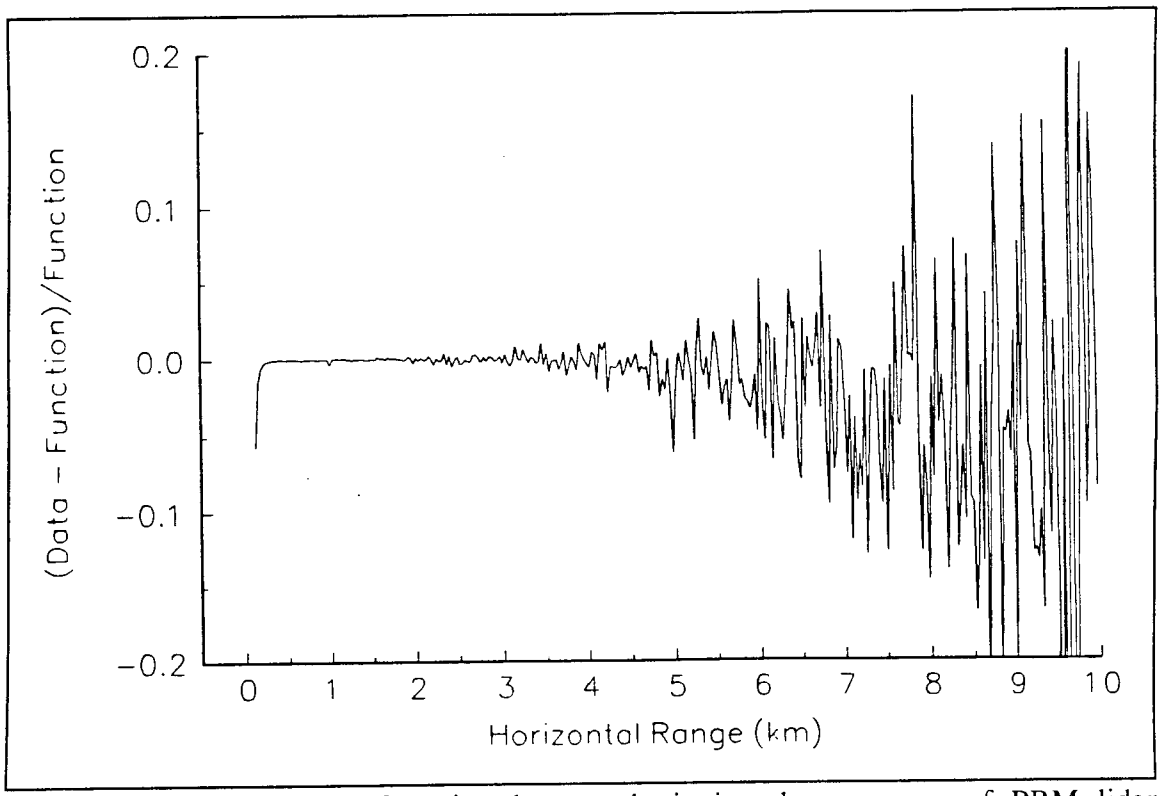

Fig. 3.1.3 Relative error of retrieved atmospheric impulse response of PRM lidar simulation. Horizontal pointing with coaxial alignment.

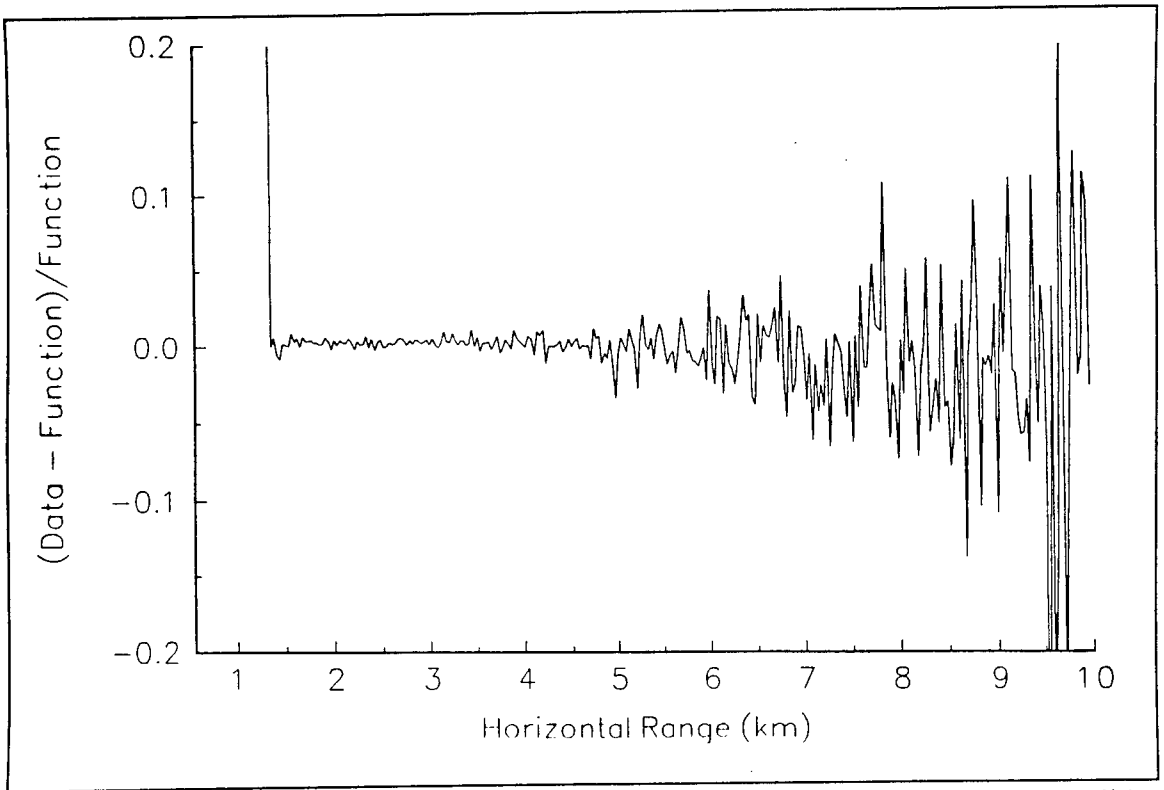

Fig. 3.1.4 Relative error of retrieved atmospheric impulse response of PRM lidar simulation. Horizontal pointing with biaxial alignment.

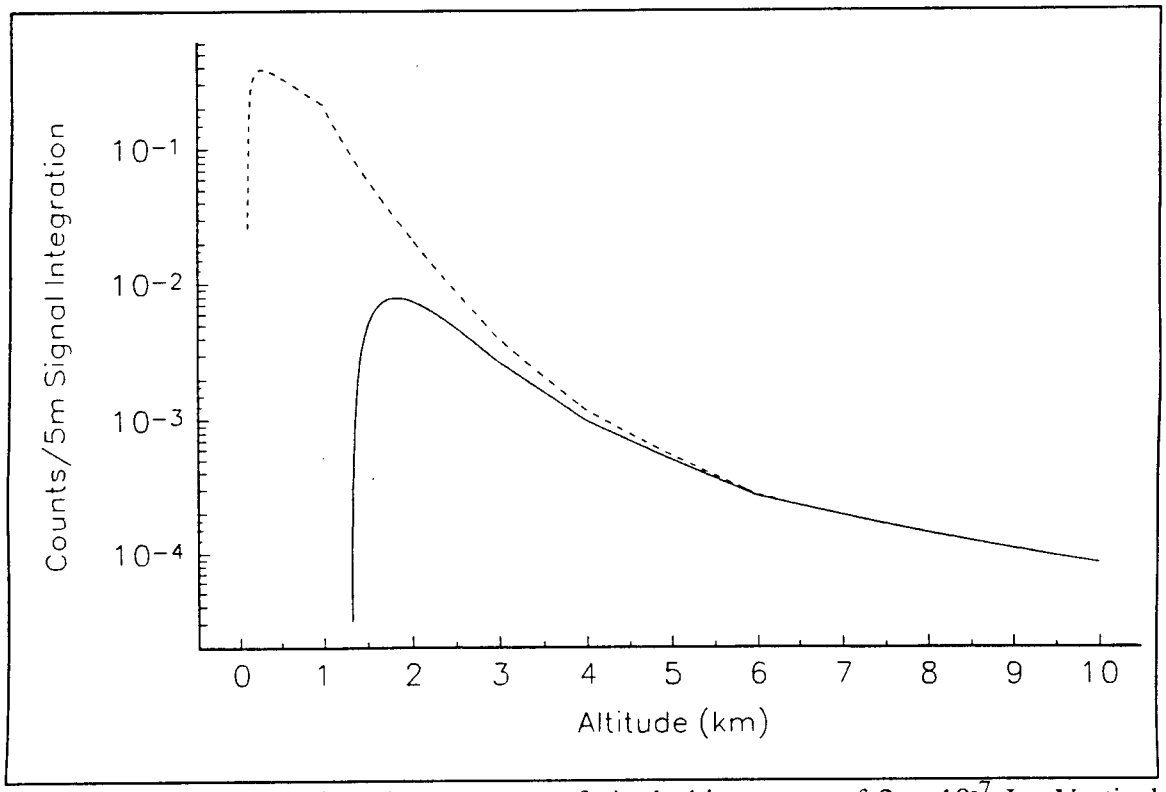

Fig. 3.1.5 Atmospheric impulse response of single bit energy of 2 x 10^{-7} J. Vertical pointing with coaxial alignment (dashed line) and biaxial alignment (solid line.)

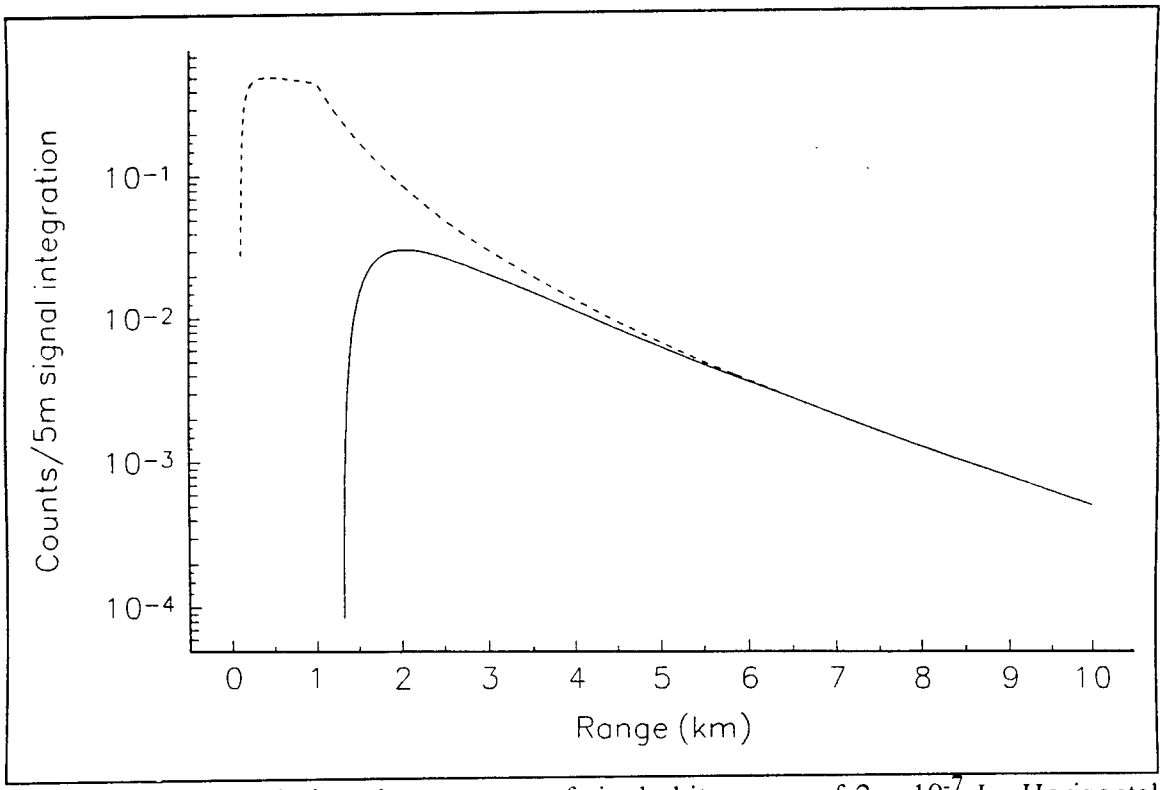

Fig.3.1.6 .Atmospheric impulse response of single bit energy of 2 x 10^{-7} J. Horizontal pointing with coaxial alignment (dashed line) and biaxial alignment (solid line.)

While reducing the average value relative to the particular value leads to some improvement in SNR at longer ranges, the overall effect is a deterioration in performance.

Table 3.1.4 shows the same result as Table 3.1.3, where the relative uncertainty is obtained through calculation of Equation 12. The results are similar to those in Table 3.1.3 obtained directly from Figures 3.1.1-4.

Tables 3.1.5 and 3.1.6 show the wind velocity uncertainties for a sample of ranges for the four situations described above. The uncertainties are given in units of m/s. The tables also show the altitude where a 1 m/s precision is obtained. The biaxial arrangement generally gives poorer performance than the coaxially one. Table 3.1.5 shows the results using a 0.1 Å FWHM spectral filter, and Table 3.1.6 assumes a 1.0 Å filter. The range for better than 1 m/s

Table 3.1.2. Simulation Parameters

Transmitter	
Power:	1 W
Wavelength:	852 nm
Divergence:	0.3 mrad
Modulation:	5 Mhz
Code Length:	511 bits
Receiver	
Aperture:	50 cm dia.
FOV:	0.5 mrad
Filter FWHM:	1.0, 0.1 Å
Day Backgrnd:	0.01, 0.001 W m^{-2} sr^{-1}
Dark Count:	5 μsec^{-1}
Filter Slope:	3.2 x 10^{-9} Hz^{-1}
Filter Trans:	0.4
Detector:	SiAPD
Atmosphere	
Aerosol Scattering Only	
Tropical Density, Temperature	
Clear Air Aerosol Model	
(~25 km Vis @ ground level)	

	Relative Uncertainty			
Range (km)	Vert-Coaxial	Vert-Biaxial	Horz-Coaxial	Horz-Biaxial
1	<0.001	N/A	<0.01	N/A
3	0.03	0.02	0.01	<0.01
5	>0.20	0.12	0.03	0.01
7	>0.20	>0.20	0.07	0.03
9	>0.20	>0.20	0.10	0.07

Table 3.1.3. Relative signal uncertainty in retrieving atmospheric impulse response estimated from PRM simulations.

	Relative Uncertainty			
Range (km)	Vert-Coaxial	Vert-Biaxial	Horz-Coaxial	Horz-Biaxial
1	0.0004	N/A	0.0002	N/A
3	0.02	0.02	0.003	0.003
5	0.29	0.16	0.015	0.009
7	0.40	0.26	0.045	0.03
9	2.4	0.79	0.14	0.08

Table 3.1.4. Relative signal uncertainty in retrieving atmospheric impulse response estimated from Equation 12.

resolution is reduced by increased ambient day background radiation for the larger bandwidth filter relative to the smaller; by 0.5 km in the vertical, and by 0.7 km in the horizontal. Nevertheless, the broader filter has a reasonably large useful range for high precision wind velocity measurement.

	Wind Velocity Uncertainty (m/s)			
Range (km)	Vert-Coaxial	Vert-Biaxial	Horz-Coaxial	Horz-Biaxial
0.25	0.05	N/A	0.05	N/A
0.5	0.06	N/A	0.05	N/A
1.0	0.09	N/A	0.05	N/A
1.5	0.31	2.9	0.13	1.1
2.0	0.85	1.9	0.26	0.47
2.5	2.1	2.9	0.45	0.56
3.0	4.8	5.3	0.74	0.71
3.5	8.5	8.8	1.2	0.96
4.0	16	14	1.7	1.3
4.5	23	20	2.4	1.8
5.0	35	28	3.4	2.3
7.0	99	73	11	6.9
9.0	176	130	29	19
1 m/s Range	2.2 km	N/A	3.5 km	3.6 km

Table 3.1.5. Wind velocity uncertainty (m/s) estimated from Equation 16, of a PRM Doppler lidar with 0.1 Å background rejection spectral filter. Last row shows range where 1 m/s uncertainty is obtained.

	Wind Velocity Uncertainty (m/s)			
Range (km)	Vert-Coaxial	Vert-Biaxial	Horz-Coaxial	Horz-Biaxial
0.25	0.09	N/A	0.08	N/A
0.5	0.11	N/A	0.08	N/A
1.0	0.16	N/A	0.09	N/A
1.5	0.59	6.7	0.21	2.4
2.0	1.6	4.4	0.42	1.1
2.5	4.0	6.7	0.74	1.3
3.0	8.9	12	1.2	1.6
3.5	16	21	1.9	2.2
4.0	30	34	2.8	2.9
4.5	45	47	3.9	4.0
5.0	67	66	5.6	5.2
7.0	184	171	18	16
9.0	329	304	48	42
1 m/s Range	1.7 km	N/A	2.8 km	N/A

Table 3.1.6. Wind velocity uncertainty (m/s) estimated from Equation 16, of a PRM Doppler lidar with 1.0 Å background rejection spectral filter. Last row shows range where 1 m/s uncertainty is obtained.

Table 3.1.7 gives the calculated uncertainty in a PRM Doppler lidar wind velocity measurement from an aircraft flying at 4 km altitude, with the lidar observing in the nadir direction. The striking feature here is the consistent result over the altitude range from near the aircraft to the ground. The higher aerosol content towards the ground compensates for the propagation scattering loss in transmission energy and $1/r^2$ dropoff, resulting in a fairly consistent figure from 2.5 km altitude to the ground. Tables 3.1.7-10 compare the expected performance for two different data accumulation periods for each of two filter FWHM. A 1 Å filter gives 1.5 m/s precision for 200 s accumulation near the ground, and close to 3.0 m/s precision at 50 s accumulation. The 0.1 Å filter gives 0.6 m/s precision at 200 s, and 3.1 m/s precision over an 8 s accumulation. Results for other accumulation times can be easily calculated, since the uncertainty goes as $1/\sqrt{t}$.

Table 3.1.8 gives the calculated uncertainty in a PRM Doppler lidar wind velocity measurement from an aircraft flying at 4 km altitude, with the lidar observing in a horizontal direction. The uncertainty increases much faster with range than in the nadir case; here the aerosol content is assumed to remain constant over the entire range at 4 km altitude. A 1 Å filter gives 1.6 m/s precision for 200 s accumulation at 1 km range, 3.2 m/s precision at 50 s accumulation. The 0.1 Å filter gives 0.5 m/s precision at 200 s, and 1.6 m/s precision over a 22 s accumulation.

	Wind Velocity Uncertainty (m/s)			
Alt (km)	1Å Nadir 200 s Accumulation	1Å Nadir 50 s Accumulation	0.1Å Nadir 200 s Accumulation	0.1Å Nadir 8 s Accumulation
3.5	1.2	2.4	0.5	2.5
3.0	0.9	1.7	0.4	1.8
2.5	1.3	2.6	0.5	2.7
2.0	1.5	3.1	0.7	3.3
1.5	1.6	3.2	0.7	3.4
1.0	1.6	3.2	0.7	3.4
0.5	1.5	3.0	0.6	3.2
0.1	1.5	2.9	0.6	3.1

Table 3.1.7. Wind velocity uncertainty (m/s) of nadir pointed, coaxial PRM Doppler lidar from an aircraft platform at 4 km, as estimated from Equation 16. The uncertainty is given for two background rejection spectral filter FWHMs: 0.1 and 1.0 Å, and for different data accumulation periods.

Table 3.1.9 gives the calculated uncertainty in a PRM Doppler lidar wind velocity measurement from an aircraft flying at 4 km altitude, with the lidar observing at a 45° angle downwards. As for the nadir pointed configuration, the signal from this configuration does not vary greatly over altitude. A 1 Å filter gives 3.1 m/s precision for 200 s accumulation near the ground, and 6.3 m/s precision at 50 s accumulation. The 0.1 Å filter gives 1.0 m/s precision at 200 s, and 2.9 m/s precision over an 22.2 s accumulation.

	Wind Velocity Uncertainty (m/s)			
Alt (km)	1Å Horizontal 200 s Accumulation	1Å Horizontal 50 s Accumulation	0.1Å Horiz. 200 s Accumulation	0.1Å Horiz. 22 s Accumulation
0.25	1.8	3.6	0.6	1.8
0.5	1.6	3.2	0.5	1.6
1.0	1.6	3.2	0.5	1.6
1.5	3.5	7.0	1.2	3.6
2.0	6.3	13	2.1	6.3
2.5	10	20	3.4	10
3.0	15	30	4.9	15
3.5	19	38	6.6	19
4.0	26	52	8.8	27
5.0	41	81	14	42
7.5	97	194	33	99

Table 3.1.8. Wind velocity uncertainty (m/s) of horizontally pointed, coaxial PRM Doppler lidar from an aircraft platform at 4 km, as estimated from Equation 16. The uncertainty is given for two background rejection spectral filter FWHMs: 0.1 and 1.0 Å, and for different data accumulation periods.

Table 3.1.10 gives the calculated uncertainty in a PRM Doppler lidar wind velocity measurement from a ground based lidar, with the lidar observing at 30° upwards. The uncertainty increases with range much faster than in the previous case, and has a large uncertainty after 4-5 km range. A 1 Å filter gives 0.13 m/s precision for 200 s accumulation at 1 km range, and 0.25 m/s precision at 50 s accumulation. The 0.1 Å filter gives 0.05 m/s precision at 200 s, and 0.14 m/s precision over a 22.2 s accumulation.

	Wind Velocity Uncertainty (m/s)			
Range [Alt] (km)	1Å 45° Down 200 s Accumulation	1Å 45° Down 50 s Accumulation	0.1Å 45° Down 200 s Accumulation	0.1Å 45° Down 22 s Accumulation
0.7 [3.5]	1.1	2.3	0.4	1.1
1.4 [3.0]	1.7	3.3	0.5	1.6
2.1 [2.5]	2.5	5.0	0.8	2.3
2.8 [2.0]	3.0	6.0	0.9	2.8
3.5 [1.5]	3.2	6.4	1.0	3.0
4.2 [1.0]	3.2	6.5	1.0	3.0
5.0 [0.5]	3.2	6.4	1.0	3.0
5.5 [0.1]	3.1	6.3	1.0	2.9

Table 3.1.9. Wind velocity uncertainty (m/s) of 45° slant path down, coaxial PRM Doppler lidar from an aircraft platform at 4 km, as estimated from Equation 16. The uncertainty is given for two background rejection spectral filter FWHMs: 0.1 and 1.0 Å, and for different data accumulation periods.

	Wind Velocity Uncertainty (m/s)			
Range [Alt] (km)	1Å 30° Up 200 s Accumulation	1Å 30° Up 50 s Accumulation	0.1Å 30° Up 200 s Accumulation	0.1Å 30° Up 22 s Accumulation
0.2 [0.1]	0.10	0.20	0.04	0.11
0.5 [0.25]	0.09	0.19	0.04	0.11
1.0 [0.5]	0.13	0.25	0.05	0.14
2.0 [1.0]	0.87	1.7	0.33	0.98
3.0 [1.5]	3.3	6.5	1.2	3.7
4.0 [2.0]	9.4	19	3.5	11
5.0 [2.5]	23	46	8.7	26
6.0 [3.0]	52	104	19	58
8.0 [4.0]	181	362	68	203

Table 3.1.10. Wind velocity uncertainty (m/s) of 30° slant path up, coaxial PRM Doppler lidar from a ground based station, as estimated from Equation 16. The uncertainty is given for two background rejection spectral filter FWHMs: 0.1 and 1.0 Å, and for different data accumulation periods.

3.2. Test Bed Experiment of PRM Incoherent Doppler Lidar Method

A simple feasibility experiment has been set up in the laboratory to perform an incoherent Doppler measurement of the speed of a rotating target. The experimental setup is depicted in Figure 3.2.1 and consists of a rotating target, solid etalon edge filter and a single mode diode laser beam. The target consists of two concentric modulation rings that are laser printed on paper. The rings impart a PRM modulation to the scattered light by a series of 255 sectors printed black for "0" bits and left white for "1" bits. The remaining 105 sectors are printed black, and the code sequence is shifted between the two rings in order to allow for simultaneous CW detection.

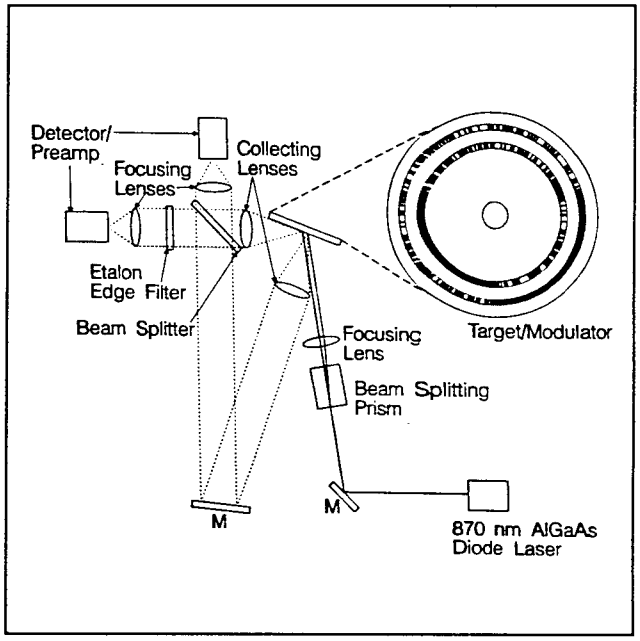

Figure 3.2.1. Test bed experimental setup.

The diode laser beam is directed to a beam splitting prism, then focused on to the two modulation rings. The scattered light from the outer ring is detected as close to the line of sight of the motion of the target as is practicable; therefore, the frequency of the light should have been Doppler shifted according to the linear speed of the target at the laser focus. The scattered light from the inner ring is collected normal to the target and is unshifted; this channel provides the reference frequency.

The signal from the rotating target is collected and collimated with lenses and is directed towards the beam splitter, which divides the light between the etalon and intensity reference channels. Because of the autocorrelation property of the PRM code, the CW signals from the outer and inner modulation rings are separable. The signals are detected and digitized, and an analysis program calculates the correlation of the data with the PRM code. The magnitude of two correlation peaks from each channel provides the intensities of: outer spot through etalon (doppler shifted), inner spot through etalon (unshifted - frequency reference), outer spot (intensity reference), inner spot (intensity reference).

After normalizing out intensity fluctuations, the frequency shift is calculated to within a constant by a simple subtraction of the normalized etalon transmission of the two spots. In the fully developed Doppler PRM system the etalon filter function slope is well characterized and provides a direct conversion from intensity difference to frequency shift.

Preliminary results show a distinct trend in the intensity difference as the speed of the target is increased. The target speed at the outer spot was varied between 2.9 m/s to 20.9 m/s, providing an expected Doppler shift of from 3.0 Mhz to 21.3 Mhz. Figure 3.2.2 shows the intensity of the reference signal and the Doppler shifted signal (lowered by the 3.0 intensity units to facilitate comparison with the reference data.) The intensity difference between reference and Doppler shows a strong bias due to the reference frequency drift, indicating that the reference frequency was in a strongly nonlinear portion of the transmission band. Figure 3.2.3 shows the frequency shift corrected for the Lorentzian line shape, and the dotted line gives a least squares fit to the data. The data were corrected by estimating the filter HWHM and frequency position of the data points (in units of Lorentzian HWHM) that provided the best fit. That the estimation provides an overcompensation is evident by comparing the trend of the reference data in Figure 3.2.2 with that in Figure 3.2.3. The most likely line shape function to describe the transmission band is a convolution of two Lorentzians, representing the filter and laser bands. Nevertheless, the correction gives a clear indication of Doppler shift from the rotating chopper.

3.3. Phase II Prototype System Design

The Phase II system design concerns largely the specific requirement of the output wavelength of the transmitter in terms of the linewidth, control and stabilization at the middle of the filter slope. The Phase II system Doppler filter will be selected based on the performance characteristics and the cost benefit. A small size solid etalon is considered as the first option for its satisfactory performance characteristics and a significant cost benefit. For the daytime operation, however, a very narrow line blocking filter will be required. The best conventional interference filters are limited to ~ 1 Å bandwidth, background-limiting the measurement range to only 3 km. An atomic filter can provide a very narrow bandwidth of up to a GHz level and is considered as a strong candidate for an operational sensor. The atomic filter technology based on the Cs line at around 850 nm range is well developed and commercially available [Menders, 1991]. Thus the proposed Phase II plan will concentrate on the basic system technology development based on a solid etalon filter. In order to adopt the atomic filter module into the

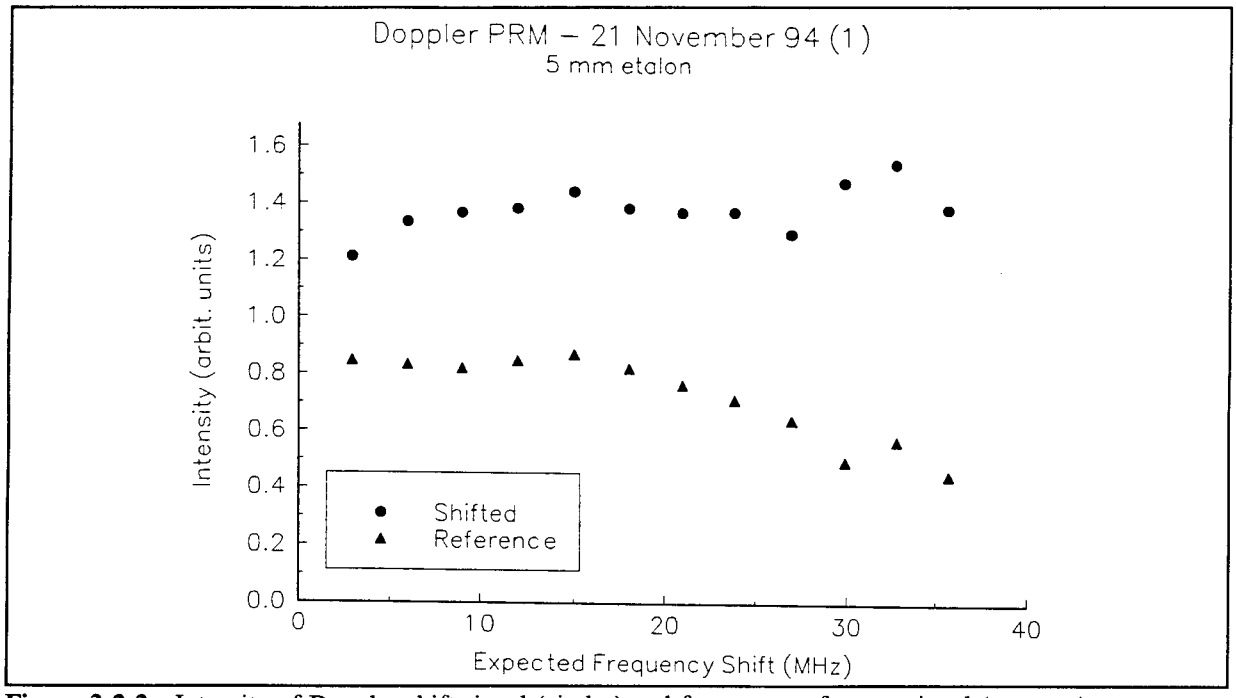

Figure 3.2.2. Intensity of Doppler shift signal (circles) and frequency reference signal (squares.)

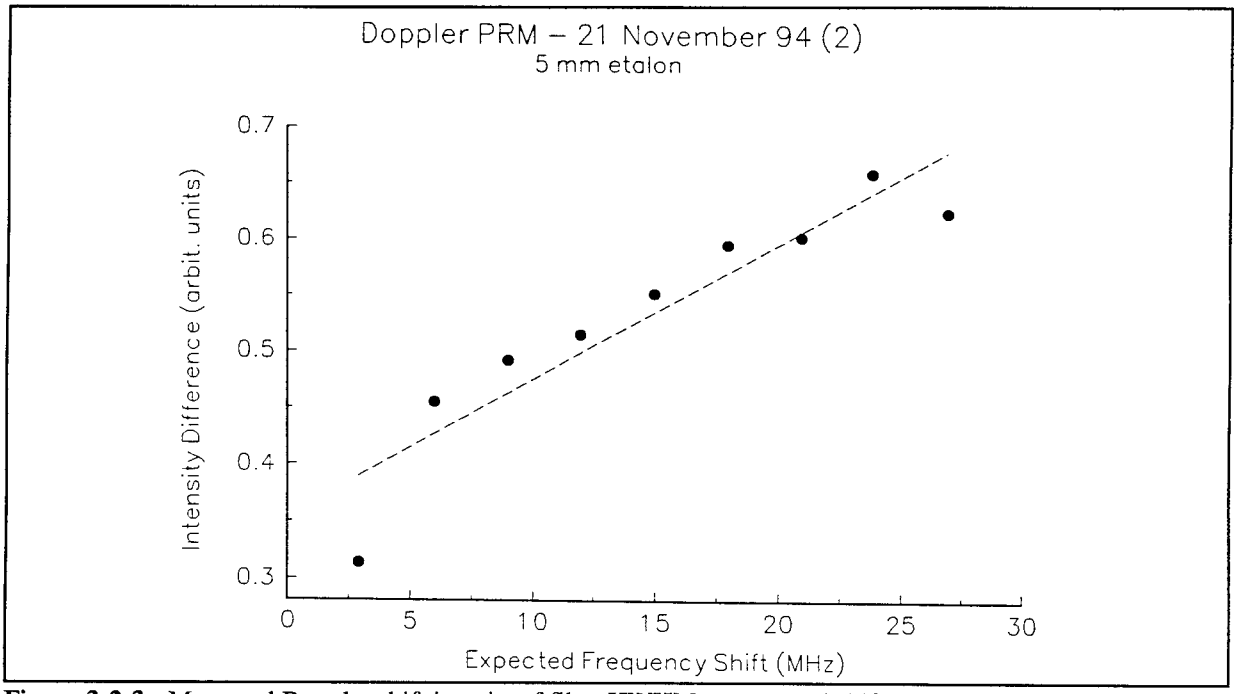

Figure 3.2.3. Measured Doppler shift in units of filter HWHM vs expected shift. Data corrected for Lorentzian band shape of etalon filter.

proposed system at the later phase of the program, we will assure the system to be tunable at around 850 nm.

3.3.1 Requirements of the Laser

An important requirement for a Doppler lidar based on the incoherent technique is for $\Delta\omega$, the linewidth (FWHH) of the laser source to be on the order of, or smaller than, the half width α at half height (HWHH), of the Doppler filter. If this requirement is satisfied then the Doppler measurement will be insensitive to the spectral width of the laser source. The two major components of the atmospheric backscattered light that is collected by the lidar receiver are: Mie scattering by the aerosols, and Rayleigh scattering by the molecular constituents of the atmosphere. The backscattered component arising from the aerosols has a narrow linewidth (corresponding to that of the laser source) while the other component due to Rayleigh scattering is much broader. For example, the Rayleigh broadening (FWHH) is about 0.03 cm^{-1} at 300 K. Because the backscattered light suffers twice the Doppler broadening, the HWHH is then about 0.03 cm^{-1}. By utilizing a narrow "edge" filter whose width is smaller than the Rayleigh broadening, only the stronger aerosol scattered light is utilized for measuring the Doppler shift, with Rayleigh scattering contributing only a broadband background. In Table 3.3.1 below, the sensitivity of Fabry Perot etalons that can be utilized as the high resolution "edge" filters for measuring the Doppler shift is given.

Table 3.3.1. Sensitivities of Etalons for Measuring Doppler Shift

Etalon Thickness, t, cm	0.2	0.5	1.0	2.0	5.0
FSR, cm^{-1}	2.5	1.0	0.5	0.25	0.1
Half width, α, cm^{-1}	4.17e-02	1.67e-02	8.33e-03	4.17e-03	1.67e-03
Resolving Pwr @ 850 nm	1.41e+05	3.53e+05	7.06e+05	1.41e+06	3.53e+06
Sensitivity (1 m/s wind), %	0.19	0.47	0.94	1.88	4.71

The sensitivity values shown in Table 3.3.1 are for a measurement at the half width point of the filter where the sensitivity is the highest. An examination of Table 3.3.1 shows that α, the HWHH of the edge filter, should be of the order of 0.0042 cm^{-1} for a 1 m/s wind measurement with a 2% sensitivity. For obtaining adequate signal to noise ratios for ranges of up to 5 km

the laser transmitter power has to be about a watt or higher.

From this it is seen that the linewidth of the laser source has to be of the order of 0.0042 cm^{-1} (125 Mhz) or better. Also its frequency has to be stable to better than 0.001 cm^{-1}. For the PRM lidar we propose to utilize a semiconductor diode laser, because of its low cost, compactness and the ease with which its amplitude can be modulated. Single longitudinal mode diode lasers with intrinsic linewidths of ~ 15 Mhz are commercially available. But when the diode laser bias current is modulated to generate the PRM code, the central frequency of laser undergoes large changes and its linewidth is also broadened considerably, thus direct application of such a laser for PRM is inadequate.

3.3.2 Methods of Frequency Stabilization of the PRM Laser

Thus the main challenge posed by the development of a PRM transmitter is the necessity to maintain the diode laser frequency constant while its amplitude is modulated at a high frequency (~ 10 Mhz) to full depth. In order for the resulting lidar to be inexpensive and rugged it is also desirable to realize this objective without adding much complexity to the transmitter. Three possible approaches for amplitude modulation of the diode laser were explored.

1. Use of an external modulator is the most direct approach. External modulation with acousto-optic or electro-optic modulators presents a simple means for generating the optical PRM code for transmission. The laser diode can then be operated at constant current and its frequency stabilized to yield the required linewidth. While this approach is attractive in view of its simplicity there are some obvious limitations. The acoustic velocity in the acousto-optic medium limits the rise time of the PRM pulses and the highest modulation frequencies lie under a few tens of Mhz. Furthermore in order to obtain a short rise time very small apertures are required leading to a limit on the power handling ability of the device. Electro-optic modulators have a much higher bandwidth and allow modulation frequencies well into the Ghz region. But, the high voltage drive required for modulating the EO devices is a serious limitation for this approach. Furthermore, the additional modulator component will require a higher system cost and further complexity of the system.
2. As mentioned above, direct modulation of the diode laser current of the conventional cleaved cavity semiconductor laser is not possible here because of the undesirable spectral characteristics. But, it is well known [Day, et al, 1993, Mooradian, 1993], that by employing a long external cavity many of the problems of frequency instability in the cleaved cavity are avoided. However in the commercial instruments available at present, either the output power is limited to a few mW, or the highest modulation frequency permitted is limited to about a Mhz, and there is an accompanying frequency change during modulation. Furthermore the external cavity lasers perform best as low power devices and need an amplifier to move into power range of a watt.
3. Injection locking the frequency of a slave laser to that of a frequency stable master oscillator is a simple and effective technique of controlling the frequency of high power lasers. This technique is widely used in solid state lasers and we have in earlier projects successfully implemented injection seeding and locking [SESI, 1993]. We propose to use this technique for

the PRM modulated high power diode laser transmitter.

Primarily the technique involves the use of a low power injection laser source whose linewidth is narrowed and is frequency stabilized to fulfil the requirements of the wind lidar. A high power broad area emitting laser diode whose current is modulated by the PRM signal is injection seeded and frequency locked to the stabilized laser. This approach has the advantages of simplicity and easy scaling to higher output power with a minimum system cost.
In the Phase I, an experimental investigation was undertaken to investigate the feasibility of the scheme and also to generate a database to help in the design of the Phase II high power PRM diode laser transmitter. Some preliminary results of the experiments that are currently in progress are given here.

3.3.3 Experimental Study of Injection Locking a Semiconductor Diode Laser

As mentioned above our approach for stabilizing the frequency of the PRM laser diode is to injection lock its output to a stable reference frequency. In the interest of simplicity, the stable frequency laser in the Phase I experiment is a single longitudinal mode low power laser diode whose frequency is stabilized passively with a low noise current supply and a precision temperature controller for holding its temperature constant.

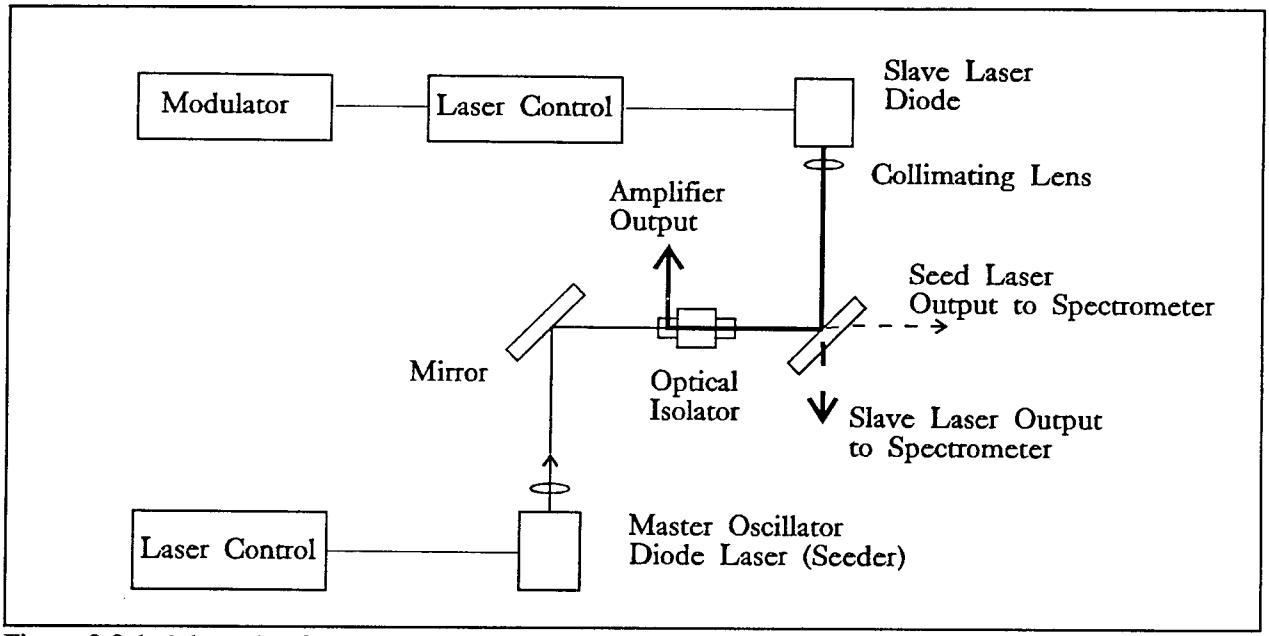

Figure 3.3.1. Schematic of the experimental arrangement for injection locking. Not shown in the figure are two apertures in front of the slave laser and photodiodes for measuring power.

Figure 3.3.1 shows the schematic of the experiment set up for studying the injection locking technique and to characterize the output of the injection locked laser. The injection seed laser

is a 30 mW commercial SLM AlGaAs diode laser (Sharp model LD 015 MD0) whose output wavelength is 843 nm at 25°C. The laser diode is mounted on a thermoelectric cooler to control its temperature. Its wavelength is controlled by a combination of changing the temperature and the bias current. The slave laser is a 100 mW commercial index guided SLM AlGaAs diode laser (SDL model AR 5412) whose output wavelength is 848 nm at 25°C. This laser incorporates a thermoelectric cooler for controlling its temperature. To permit this laser to be utilized as an amplifier and to utilize an external cavity when required, the front facet of the slave laser is antireflection coated to reduce the normal reflectivity of the cleaved facet from about 4% to 0.5%. The back facet which forms the rear reflector of the laser cavity retains its normal 95% reflectivity. It may however be pointed out that the residual reflectivity of the front facet is still fairly high and causes the diode to lase at a fairly low threshold current. Custom anti-reflection coatings that yield much lower reflectivities are essential for increasing the laser threshold, so that high level of amplification can occur.

An optical isolator is placed in between the two lasers to allow the seed laser light to fall on the slave laser but to block the light in the reverse direction. Two optical isolators, each consisting of two polarizers with a Faraday rotator in between were placed in tandem to obtain adequate isolation (about 50 dB). Each isolator rotates the polarization axis by 45°, and hence the directions of polarization of the seed and slave laser are rotated at 90° to each other. For our experiments a grating spectrometer is utilized as the main diagnostic tool in addition to a photodetector for measuring the output power. A 1 meter Czerny Turner spectrometer with a resolution of 0.01 nm, is equipped with a photodiode array to yield a dispersion of 0.02 nm / pixel. Three different sets of preliminary experiments on injection seeding have been performed with this setup and the results are shown below. The spectra shown below were all acquired with 10 msec of integration time, and are the average of 50 such spectra.

3.3.3.1 Injection Locking of CW Laser

In the first series of experiments the 100 mW slave laser was injection locked to the 30 mW seed laser. Since the wavelengths of operation of the master and slave diodes at 25°C were considerably different (843 and 848 nm), the slave laser was cooled by about 30 K (temperature coefficient ~.2 nm/K) and was run at -5 to -7.5°C. The master laser was run at about 20°C. It was found that the slave laser was easily injection locked for a range of operating currents for both master and slave laser. When the master laser was operated at 65 mA and the slave at 95 mA the wavelength difference was about 3.5 nm. Injection locking occurred but tended to be unstable with the slave laser falling out of lock on occasions. But when the power of the master laser is increased, locking was very effective and at 75 mA locking occurred at all situations. At 65 mA, the output from the diode is about 11 mW and about a quarter of this power (2.66 mW) is incident on the collimating lens in front of the slave laser. The beams from both the lasers were not circularized (no anamorphic prisms were used) and nearly 40% of the output was lost in the apertures. Thus it is estimated that about 15% of the power from the seed laser was incident on the slave laser. From this estimate, about 1.6 mW of seed power is incident on the slave laser at 65 mA of bias current, 2.7 mW at 75 mA of current, and 3.9 mW at 85 mA.

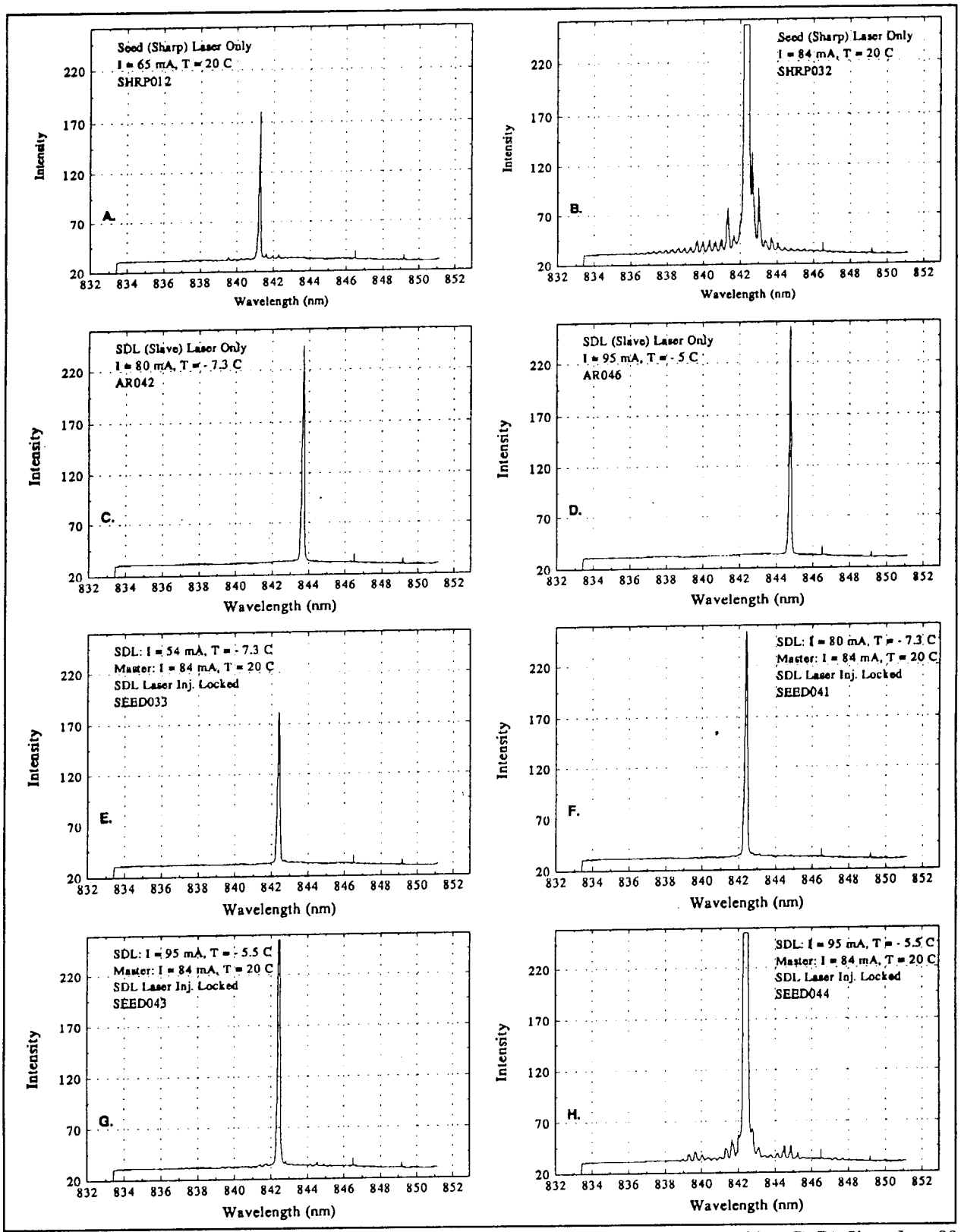

Figure 3.3.2 Spectra of diode lasers. A) Seed I = 65 mA B) Seed I = 84 mA mag 20x C) D) Slave I = 80 mA, 95 mA E) F) G) Injection locked slave I = 54, 80, 95 mA H) G mag 20x.

When the alignment was improved, consistent locking occurred at less than 500 μW of seed power.

In Figure 3.3.2 several spectra of the injection locked (E, F, G, and H) slave laser are shown. Also shown are the spectra of the master (seed) laser (A, B). The spectrum of the master laser has been magnified (x20) to show the presence of many longitudinal modes. With increasing current the number and magnitude of the side bands is reduced. At 85 mA, the magnitude of the strongest side band modes was about 0.5 % of the central mode. The free running slave laser spectrum is found to be similar (C, D). The spectrum of the injection locked slave laser shows that the slave laser mode is pulled into the master laser mode. Also observed is that the output spectrum is similar to that of the master although the intensity of the side bands is much reduced.

Locking occurred over a wide range of slave laser powers, as seen in E, for a slave laser current of 54 mA, (power = 26 mW), F (I = 80 mA, 51.3 mW) and G (I = 95 mA, 65.9 mW), and over a range of temperatures, from -10 to -5.1°C. Injection lock was lost at > - 5°C, but was recovered by wavelength tuning the master laser.

3.3.3.2 Injection Locking of Modulated Laser

A second series of experiments was performed wherein the slave laser amplitude was modulated by modulating its bias current. A 4 kHz square wave was fed into the external analog input of the slave laser power supply (SDL Model 800). The modulating signal is summed with the bias current and supplied to the laser diode. The bias level was changed to vary the depth of modulation from full depth (20 to 95 mA), to 50% depth (55 mA to 95 mA).

Figure 3.3.3 shows the spectra of modulated slave laser. Modulation of the laser current causes the spectrum to broaden as seen in A and C, where additional longitudinal modes are seen. In A, the bias current is below the threshold, so that during the off state of the modulation the laser is turned off, whereas in C the bias current is much above threshold. In both B and D it is observed that the injection seeding locks the output of the modulated laser to that of the seeder. In D, however there is a slight increase in the background. A high resolution scan of the spectrum is necessary to examine if the line width of the laser is broadened. Further experiments are planned to measure the line width.

3.3.3.3 Power Amplifier

If the slave laser is used as a simple power amplifier the output will not be influenced by the characteristics of the slave laser resonator. For utilizing the slave laser as an amplifier, the gain of its resonator has to be very low so that self oscillations are held off, and only the master oscillator wave is amplified. With this goal in mind the slave laser front facet is anti-reflection coated. But as mentioned above the residual reflectivity is still high ($\sim$0.5%), so that the threshold current for lasing is fairly low ($\sim$25 mA). Amplification of the seed laser was

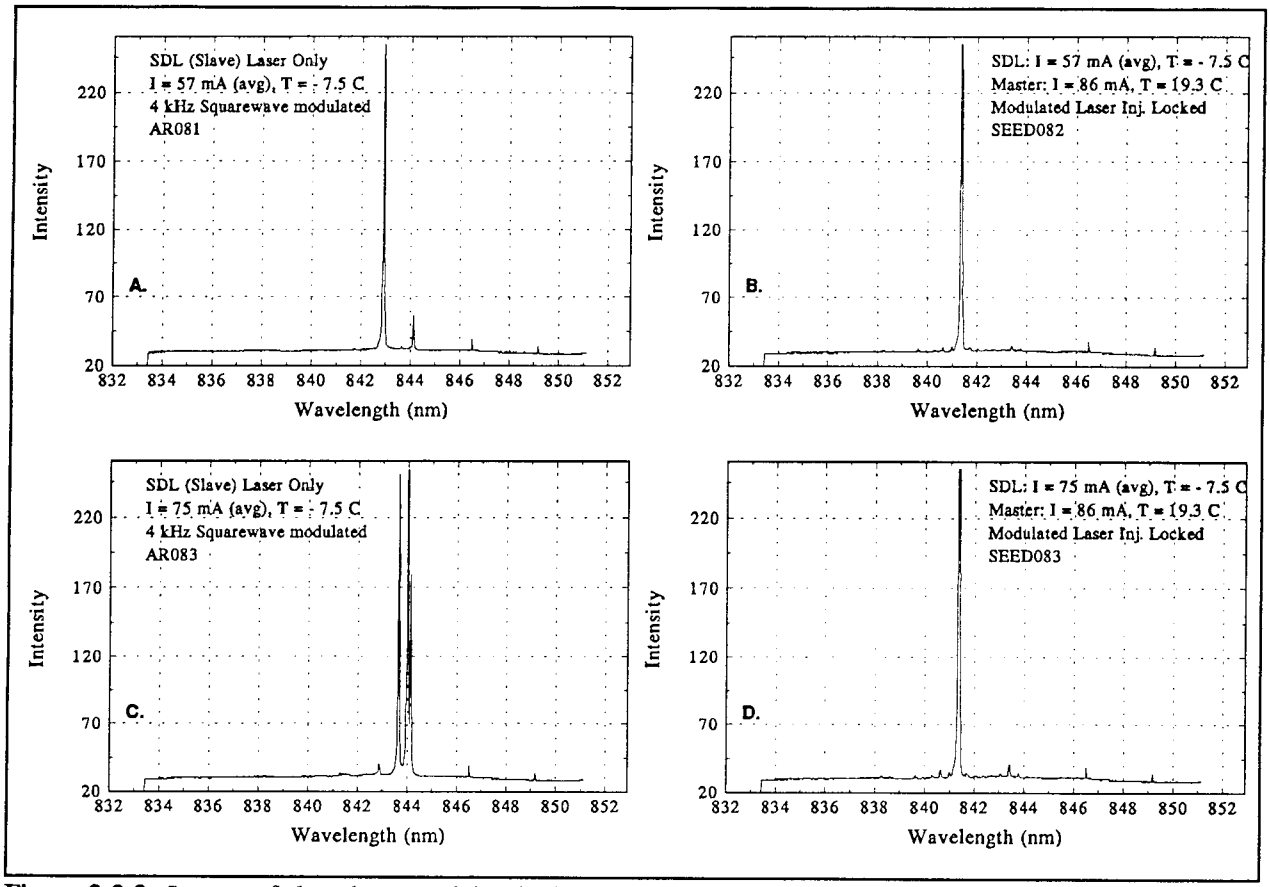

Figure 3.3.3. Spectra of slave laser modulated with 4 kHz square wave. A) Free running diode, 100% mod. B) Injection locked, 100% mod. C) Free running, 50% mod. D) Injection locked, 50% mod.

observed at current levels below the threshold. Figure 3.3.4 shows the results of this experiment. It is seen that amplification occurs below 25 mA of bias current.

The master laser input power is about 3.9 mW. Sufficient gain can be obtained by reducing the reflectivity further so that much higher levels of amplification can result. The spectra of the amplifier corresponding to these experiments are shown in Figure 3.3.5. The amplifier spectra are found to be exact reproductions of the master oscillator spectra. The amplifier thus presents an extremely useful configuration to obtain a high power PRM laser source.

3.3.4. PRM Laser Transmitter

The results of the preliminary experiments presented above have shown that injection locking of a high power diode laser is accomplished very effectively with a few milliwatts of seed laser power. Such injection locking occurs even when the slave laser is modulated over the full depth. The modulation frequency used in the preliminary experiment, however, is low and additional experiments with high frequency modulation as well as high resolution measurements of the linewidth are planned.

Hence the transmitter proposed for the Phase II system consists of a high power broad area

AlGaAs laser diode with output of about 1 W. A low power (10 - 20 mW) AlGaAs external cavity stabilized single longitudinal mode tunable diode laser with a linewidth of ~15 Mhz, and a frequency stability of the order of 15 - 20 MHz over 15 minutes or longer, will be used as a master oscillator. Such external cavity tunable diodes are available commercially (New Focus) and are well suited for our requirement.

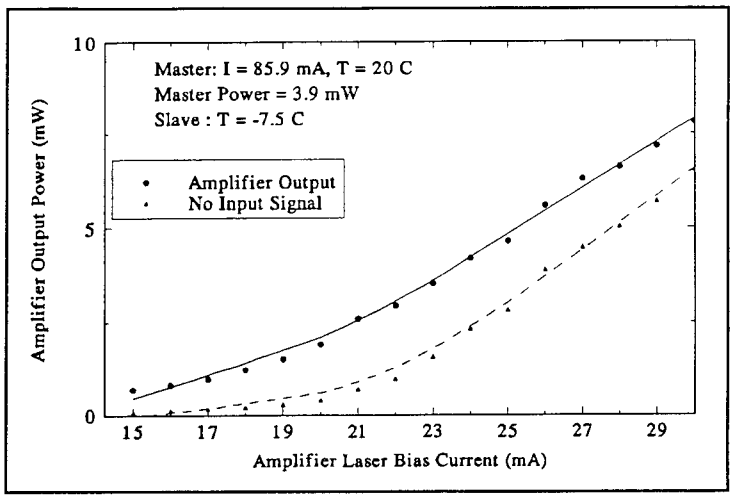

Figure 3.3.4. Output of the AR coated laser diode. The solid line indicates amplification of master laser input.

Although it was shown that amplification of the master oscillator yields spectral characteristics of the output that are virtually identical to that of the master oscillator, for obtaining sufficient power output, high gain operation of the amplifier without self lasing is necessary. Successful development of such an amplifier is predicated upon the successful development of extra low reflectivity coatings for the high power laser diode.

3.3.4.1. Frequency Stabilization

Use of an external cavity for continuously tuning semiconductor lasers, for stabilizing its frequency, and for linewidth narrowing is well known [Mooradian, 1993, Day, et al, 1993]. Demonstrations of such systems with ultra narrow linewidths and frequency stability (< 1 Mhz) for low power and even high power (>100 mW) are documented in the literature [Kakiuchida, etal, 1994, Sharfin, et al, 1989]. Currently commercial devices with output powers of 10 mW and narrow width (< 5MHz over 5 s) are readily available. The output frequency of the seed laser will be tuned such that the transmission through the Doppler "edge" filter is approximately 50%, such that it corresponds to the optimum sensitivity of the edge technique. By monitoring the transmission with a photodiode it is easy to tune the seed diode laser frequency such that the transmittance is maintained constant at near 50%.

3.4 Phase II Prototype System Configuration

The sensor system consists of three sub-systems: the diode laser transmitter/scanner, the receiver/detector, and the signal processing electronics including a computer (PC). In the baseline mode, the diode laser transmitter is digitally modulated by a 10 MHz pseudo-random code of a given length (1024) to provide a 15 m quantization precision and 15 km unambiguous range coverage. The receiver optics consist of a 0.5 m diameter telescope, an edge filter, and a pair of detectors. The output of the detector/preamp signal will be further amplified before

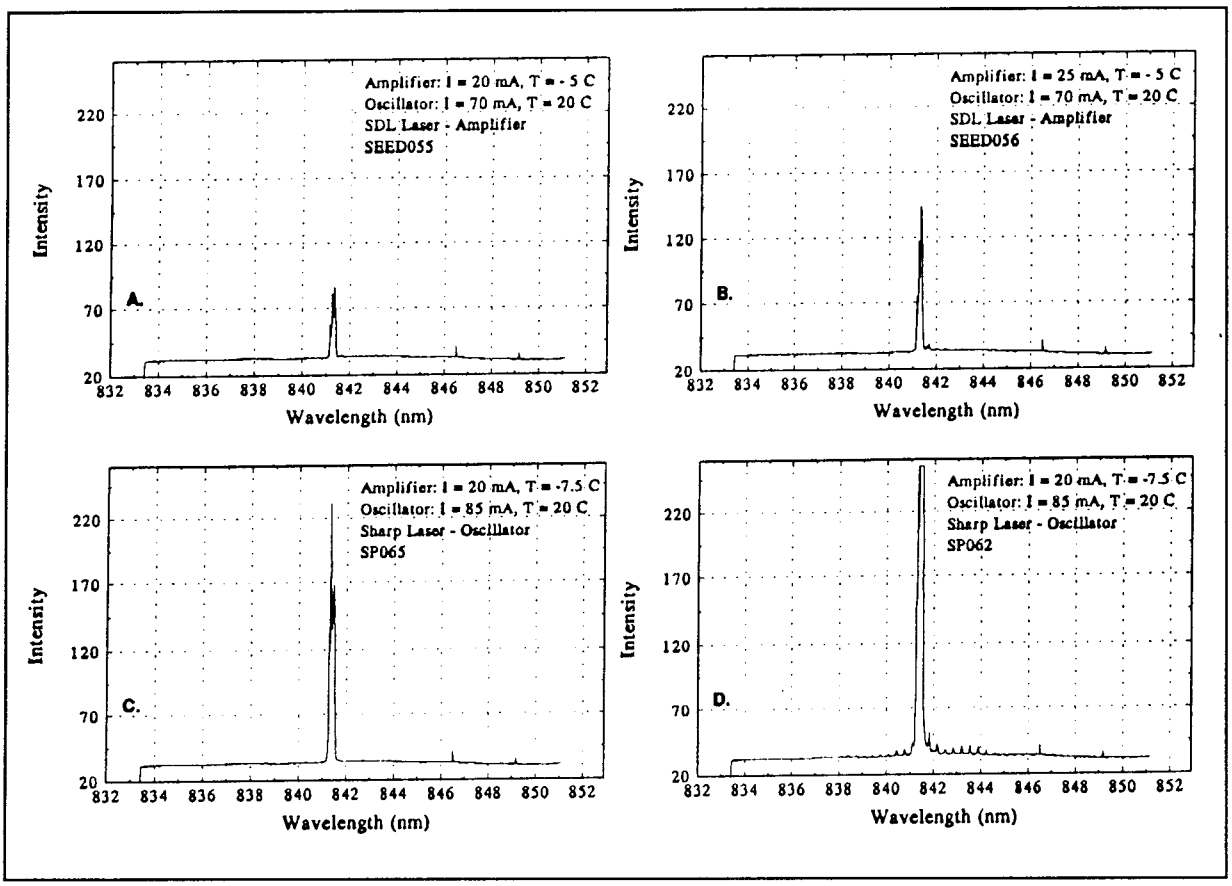

Figure 3.3.5. Spectra of the power amplifier. A. Free running diode laser, 100% modulation; B. Injection locked. C. Free running diode, 50% depth of modulation; D. Injection locked.

the photon counting detection. The digital photon counter signal will be accumulated for signal integration. An order of 200 sec integration time will be required for a 1 m/sec velocity resolution. The output of the integrated signal will be sent to the cross correlator and signal processing computer for range resolved wind velocity measurement. The correlation operation and wind velocity measurement will be carried out by the system computer. We propose to integrate a DSP chip to increase the speed of the correlation calculation.

According to the simulation result, the biaxial configuration with a large cross over distance does not provide a significant benefit compared to the coaxial configuration performance except for a small gain in the range coverage at a large distance. Therefore the Phase II prototype will be based on a coaxial configuration which will provide the data from the near field without any dead space.

3.4.1 Receiver

A Phase II prototype will be based on a 0.5 meter diameter receiver. The FOV of less than 1 mrad will be implemented for an effective background signal suppression. An optical

interference filter with 1 Å FWHM will be employed in the Phase II system, with a capability of further upgrading in commercial unit using the atomic filter. A manual scanning capability will be provided in the prototype system.

Table 3.3.2. Baseline Transmitter

High Power Slave AlGaAs Laser Diode	
Power	1 W
Wavelength	810 nm
Linewidth	200 MHZ
Frequency Stability (15 min)	50 MHz
Modulation (TTL input)	20 MHz
Modulation Depth	50 - 100%
Low Power Seed AlGaAs Laser Diode	
Power	10 mW
Wavelength	810 nm
Linewidth	15 MHz
Frequency Stability (15 min)	20 MHz
External cavity frequency stabilized laser.	

3.4.2 Doppler Filter

A Fabry-Perot etalon is proposed as the edge filter in the Phase II prototype system. An etalon with a transmission Lorentzian line shape of 250 MHz full width half maximum (FWHM) is deemed suitable for high resolution wind velocity measurements. Figure 3.4.1 shows the transmission function of an interferometer with a 2 cm air gap, or equivalently for a solid etalon 1.33 cm thick, with an index of refraction of 1.5. The reflectivity is 95% and the scattering and absorption losses are estimated at 0.2%. The finesse of the etalon is 30. The filter transmission gradient at half maximum (T=0.46) is 4 x 10^{-9} Hz^{-1}, which, according to the simulation, is a sufficiently high value in providing high sensitivity measurements of the wind velocity.

3.4.3. Detector

For compactness and high quantum efficiency at the near ir wavelength, we will implement a Geiger mode SiAPD detectors available commercially. The after pulsing effect of the detector in the visible range is expected to be negligible with the near ir used in this system [Lee, 1989; 1990]. The photon histogram counter will be implemented on an IBM PC prototype I/O board which is to acquire photon counts from the detector over a programmed period of time or a number of PN-code cycles. The photon counter can run at 10 MHz or a lower speed. It will provide a large dynamic range with a maximum channel length of 4095. There is no dead time between bins and cycles. The concept relies on a double memory buffering technique to provide a large dynamic range. In this concept, while

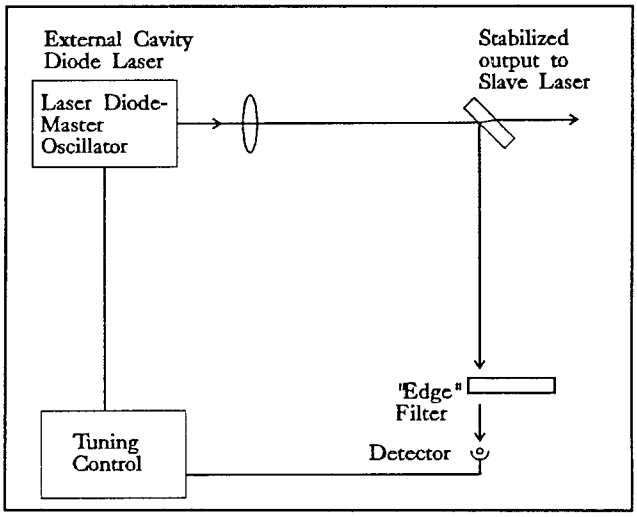

Figure 3.3.6. Layout of scheme for adjusting the frequency of diode laser master oscillator.

one buffer is counting the detected photons, the processor fetches the data from the other buffer. Each buffer memory has a length of 4095 locations. The photon counter requires an external clock common to the system clock. The period of the clock defines the time resolution and the clock rate could be varied. An external trigger pulse starts a new counter cycle on a rising edge, incrementing only one count for each time bin. At a given time, one of the two memory buffers is engaged in photon counting. If one or more locations of buffer memory reaches the counting limit (8-bits, 256 counts), the system will switch on the cleared memory buffer to take over the counting function. At the same time, the system will set the "Full-Count" flag to the computer. The computer then starts to fetch data from the non-counting buffer memory. The fetched data is added to the accumulated program memory. The recently-read buffer memory will then be cleared and ready to acquire data. This design enables an unlimited depth of accumulation. The on-board circuitry will be designed to buffer the Input/Output lines and provide address coding. The software will monitor the flags of the counter board and control the traffic of the buffer memories. The software program will also acquire data and store it in a file format on a hard disk. The data will be accumulated by an efficient digital adder [Tausworthe et al, 1990] for the duration of the integration. The output of the adder will then be transferred into the buffer memory, which the computer will access for correlation calculation and further signal processing.

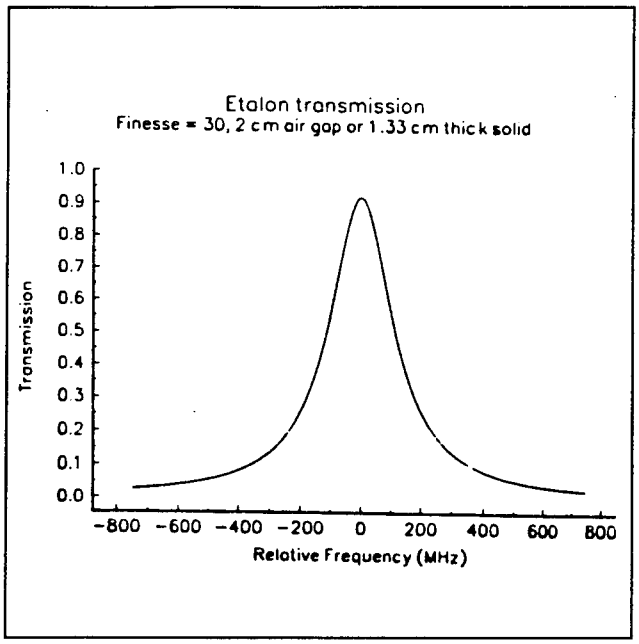

Figure 3.4.1. Transmission for 1.33 cm thick etalon, of finesse = 30. FWHM = 250 MHz.

3.4.4 Electronics System

The sensor electronics subsystem consists of three sub-systems: the transmitter; the analog front-end subsystem; and the signal processor. The transmitter consists of a PN code generator, the diode laser with associated drive circuits, and the interface circuits. The analog front-end consists of the detectors, preamplifiers, and the signal conditioning module for photon counting and digitization. The signal processor accumulates and processes the digital data to extract the range resolved wind velocity calculation. SESI's previous experience in developing an AlGaAs Altimeter Histogram photon counter (the photon counter board counts one or no photon in each clock period which is equivalent to a one-bit digitizer) will be fully utilized for the present application.

3.4.5 Signal Processing

The signal from the photon counting will be accumulated by an efficient digital accumulator [Tausworthe et al, 1990] for the duration of the integration. The output of the accumulator will then be transferred into the buffer memory which the computer will access for correlation calculation for the wind velocity measurements. To extract the wind information in a limited time, several high speed digital signal processors (DSP), such as the AT&T 3210 (operating at 66.6 MHz) will be considered for use. Each DSP will be configured to receive and process the data sequentially from the detectors, resulting in a substantial reduction of processing time. The data can then be stored and transferred to a graphics system.

4. Potential Post Applications

The cost effectiveness, robust performance for intermediate range wind profiling, and the real time field operational capability provide a significant potential for commercial applications.
The Phase I results assures the availability of the cost effective high power PRM laser transmitter consisting of a high power semiconductor laser system. Techniques for implementation of the transmitter with a high sensitivity Doppler filter in a cost effective manner have been identified and are being developed based on an inexpensive solid etalon. The data system and signal processing algorithms were developed and tested in Phase I. An extensive simulation model results, based on these system parameters and conservative field conditions, demonstrate the system capability of wind measurement up to 5 km for both the day and night time operations.
Some potential applications of this sensor are discussed below:

i) Avionic Safety Control - The avionic safety in terms of the atmospheric turbulence and micro-burst will be readily addressed with this system in a cost effective and robust manner. A ground based maintenance free operation will be realized due to the unique system characteristics of small, lightweight, low power consumption and negligible maintenance requirement.

ii) Battlefield Weather Nowcast - Standoff detection for biochemical warfare requires a nowcast capability with a significantly high resolution and sensitivity. Wind field information is one of the most important parameters for such a mesoscale circulations associated with the tropospheric dynamics. Such a wind measurement capability is also required for accurate trajectory calculation for the realtime battlefield applications.

iii) Aerosol Measurement - The byproduct data of the sensor is the high resolution aerosol profile which will be very useful for the battlefield detection of the aerosols importance of military applications.

iv) Range Doppler Laser Radar - A compact and powerful lidar system for range-Doppler measurements of hard targets will be very useful for military applications as well as for avionic

collision avoidance applications.

5. Conclusions

In the conventional lidar systems, the transmitter is characterized by a high power pulse laser to accomplish a required range-Doppler resolution. In the pulse system, although the peak power of the transmitter is very high, the average power is only a few watts due to its low repetition rate. This average power is comparable to the average power of the proposed cw PRM diode laser radar transmitter. In principle, therefore, the proposed system should be capable of measuring wind velocities at large distances. However, an extensive system analysis and simulation study in Phase I shows that the actual system performance does not quite scale up linearly with the average power. The return signal of a PRM lidar is a summation of the signals originating from the distributed scattering sources. Thus the S/N ratio is governed by the photon statistics of the net return signal. Consequently the range capability of the PRM lidar system is somewhat limited compared with the pulse system. With this limitation, a practical PRM lidar system will profile the wind nominally up to 5 km range with a meter per second resolution.

With this limitation the PRM wind lidar, regardless the transmitter output power, can not address a very long range applications such as spaceborne measurements or an high altitude measurement. In spite of this limitation, the PRM wind lidar concept remains to be very practical for many operational uses including the avionic as well as defense applications. The system will provide a high resolution, high speed wind profile within a 5 km range which will cover most of the now forecast and hazardous environment detection capability critically required for numerous situations. The PRM system can address a number of practical issues of the deployment of the lidar systems in the field, including portability, power and maintenance requirement as well as the cost requirement. These merits of the system configuration offsets the limitations of the range capability and provides a significant commercial potential. Further development effort in Phase II will provide the performance data necessary for the commercialization of the PRM lidar system.

References

Day, T., F.Luecke and M.Brownell, "Continuously tunable diode lasers", Lasers and Optronics, 15, June 1993.

Kakiuchida, H., and J. Ohtsubo, "Characteisitics of a semiconductor laser with external feedback", IEEE J. Quantum Electronics, **QE-30**, #9, 2087-2097, 1994.

Lee, H. S., C, Prasad, G.K. Schwemmer, and T.R. Glesne, "Optimum Parameters for Injection Seeding of a Tunable Solid State Laser", Proceedings of CLEO 1991, Parer No. 0349, May 12-17, 1991.

Lee, H.S., and R. Ramaswami, "Study of pseudo noise diode laser for ranging applications," SPIE Vol.1829, Cooperative Intelligent Robotics in Space III, pp36, 1992.

Menders, J., K. Benson, C. S. Liu, and E. Korevaar, "Ultranarrow line filtering using a Cs Faraday filter at 852 nm," Optics Letters, Vol. 16, No.11, pp846-848, June, 1991.

Mooradian, A., "External cavity tunable diode lasers", Lasers and Optronics, 35, May 1993.

Nagasawa, C., M. Abo, H. Yamamoto, and O. Uchino, "Random modulation cw lidar using new random sequence", Applied Optics, Vol.29, No.10, pp1466-1470, April, 1990.

SESI, "Development of systems for continuous tuning and single mode operation of solid state lasers, NASA SBIR Phase II Final Report, NAS 5-30857, 1993

SESI, "A diode pumped, broadly tunable, actively stabilized, single mode, LiSAF laser, NSF SBIR Phase I Final Report, #9360950, 1994.

Sharfin, W.F., J.Seppala, A.Mooradian, B.A.Soltz, R.G.Waters, B.J.Wollmer and K.J.Bystrom, "High-power diffraction-limited, narrow-band, external-cavity diode laser", Applied Physics Letters, **54**, #18, 1731-1733, 1989.

Takeuchi, N, and K. Samurai, "Lidar system using pseudo-random code modulation", Proc. Int. Laser Radar Conf.,San Candido, Italy, June 20-24, 1988.

Tausworthe, R. C., and J. R. Smith, "Simplified correlator for ranging codes", NASA Tech Briefs, pp36-38, May, 1990.